Available online at www.sciencedirect.com
ScienceDirect
Journal of Power Sources 184 (2008) 583–588
JOURNAL OF POWER SOURCES
www.elsevier.com/locate/jpowsour

Short communication

Electrochemical study on $LiCo_{1/6}Mn_{11/6}O_4$ as cathode material for lithium ion batteries at elevated temperature

H. Huang, C. Wang, W.K. Zhang *, Y.P. Gan, L. Kang

College of Chemical Engineering and Materials Science, Zhejiang University of Technology, Hangzhou 310032, China

Received 28 November 2007; accepted 12 December 2007
Available online 23 December 2007

Abstract

A novel process via sintering of a precursor from the solution of metal acetates by spray-drying technology was used to synthesize Co-substituted $LiCo_{1/6}Mn_{11/6}O_4$ material for lithium ion batteries. The as-prepared particles were identified as single-phase spinel structure without any impurities in the XRD pattern. The SEM image showed that the particles had good cubic shapes and uniform size distribution with sizes of about 100–200 nm. An ex situ XRD technique was used to characterize the first charge process of the $LiCo_{1/6}Mn_{11/6}O_4$ electrode. The result suggested that the material configuration maintained invariability. The electrochemical properties of the synthesized cathode material were investigated using Li-ion model cells at room and elevated temperature, respectively. In the charge/discharge potential of 3.5–4.4 V at 1/10 C rate, the $LiCo_{1/6}Mn_{11/6}O_4$ electrode delivered high initial capacities of 123 and 127 mAh g^{-1} at 25 and 55 °C, respectively. Electrochemical cycling tests revealed that the capacity fading occurred mainly in the high-voltage region of 4.08–4.40 V, and the fading rate was 0.107% and 0.302% per cycle at 25 and 55 °C, respectively. The excellent cycling stability and low material cost make it an attractive cathode for high-temperature lithium ion batteries.

Keywords: Spinel $LiCo_{1/6}Mn_{11/6}O_4$; Spray-drying method; Ex situ XRD; Electrochemical properties

1. Introduction

As power sources for electric vehicles and hydride electric vehicles (EV and HEV), lithium ion batteries are usually limited in widespread commercialization by poor cycling characteristics at the elevated temperature. The high-temperature performance of lithium ion batteries is directly associated with cathode materials. Over the past 20 years, spinel $LiMn_2O_4$ has been investigated extensively and considered as a promising cathode material due to its low cost, less toxicity and high thermal safety [1–3]. Nevertheless, $LiMn_2O_4$ shows problems related to poor cycling behavior because of a fast capacity fade in 3 V region due to the phase transformation from cubic structure to tetragonal structure, and also in 4 V region resulting from Mn (Mn^{3+}) dissolution during lithium ion insertion/extraction [4,5].

So far, great efforts have been made to alleviate the capacity loss of $LiMn_2O_4$ during cycling, one of which is to substitute a small portion of Mn ions by other metal ions. The substituted manganese spinels $LiM_xMn_{2-x}O_4$ (M = Co, Ni, Cr and Al) showed a significant improvement on the cycling properties over the parent $LiMn_2O_4$ [1,6–9]. Among them, $LiCo_xMn_{2-x}O_4$ has been especially concerned of its stabilized structure and reduced strain during the repeated insertion/de-insertion of lithium, which makes it one of the most promising materials for practical use. However, the initial specific discharge capacity of $LiCo_xMn_{2-x}O_4$ decreases monotonically with the increasing of Co-substituted content. Different Co-contents were suggested in preparing $LiCo_xMn_{2-x}O_4$ spinels via various preparation methods [10–12]. Shen et al. reported that $LiCo_{0.1}Mn_{1.9}O_4$ showed the best cycling performance among $LiCo_xMn_{2-x}O_4$ spinels (x = 0–0.5) by conventional solid-state reaction, with initial discharge capacity of 105.4 mAh g^{-1} and capacity loss of 0.48% after 20 cycles [13]. Wu et al. utilized a Pechini process for synthesizing $LiCo_xMn_{2-x}O_4$ spinels (x = 0–0.5), and the results showed that $LiCo_{0.2}Mn_{1.8}O_4$ exhibited the best cycling performance with initial discharge capacity of 110 mAh g^{-1} and fading rate of 0.45% per cycle [14]. It is inferred that the optimum Co-content in the $LiCo_xMn_{2-x}O_4$ spinel was between 0.1 and 0.2.

* Corresponding author. Tel.: +86 571 88320394; fax: +86 571 88320394.
E-mail address: msechem@zjut.edu.cn (W.K. Zhang).

0378-7753/$ – see front matter © 2007 Elsevier B.V. All rights reserved.
doi:10.1016/j.jpowsour.2007.12.043

For the battery application, $LiM_xMn_{2-x}O_4$ powders should possess single-phase, homogeneity, uniform particle morphology with submicro-sized distribution for achieving good electrochemical properties [15,16]. However, it is difficult to control such factors using a conventional solid-state reaction, because this process requires a prolonged heating treatment at high temperature with the repeated intermediated grinding [8,17,18]. Recently, a facile spray-drying process has been introduced to synthesize $LiMn_2O_4$ material. The advantages of the approach lie in the facts that the particle size is narrowly distributed; the composition and morphology can be easily controlled. Using a spray-drying technology, Wu et al. succeeded in synthesizing $LiMn_2O_4$ compound with excellent electrochemical properties [19,20]. In this work, the submicro-sized $LiCo_{1/6}Mn_{11/6}O_4$ spinel with high homogeneity and uniform particle morphology was prepared successfully by a spray-drying method. The crystal structure, morphology and elevated temperature properties of the products as cathode material for lithium ion batteries were investigated. And an ex situ XRD technique was used to characterize the structure stability of the $LiCo_{1/6}Mn_{11/6}O_4$ material.

2. Experimental

Stoichiometric amounts of $CH_3COOLi{\cdot}2H_2O$, $Mn(CH_3COO)_2{\cdot}4H_2O$, $Co(CH_3COO)_2{\cdot}4H_2O$ were dissolved in distilled water. Metal acetates were measured with molar ratio (Li:Co:Mn = 1:1/6:11/6). The resulting solution was dried to form a mixed dry precursor via a spray-dryer. The solution was atomized via a sprinkler at an air pressure of 0.2 MPa and was spray-dried by hot air. The inlet air temperature was 220 °C, and the exit air temperature was 110 °C. The as-prepared precursor was sintered at 400 °C under an oxygen atmosphere for 4 h then the obtained products were ground in an agate mortar and re-sintered at 700 °C for 12 h. The morphology and size of the particles were observed using a scanning electron microscopy (SEM, HITACHI S-4700 Π). The phase identification of the products was carried out by powder X-ray diffraction (XRD, Philips PC-APD) using Cu Kα radiation.

A slurry consisting of $LiCo_{1/6}Mn_{11/6}O_4$ powder, acetylene black as the conducting agent, and polyvinylidene fluoride as the binder was pasted onto an aluminum foil. The weight ratio of $LiCo_{1/6}Mn_{11/6}O_4$ active powder, conducting agent and binder was 80:10:10. The pasted electrode was dried in air at 80 °C for 4 h, and pressed at a pressure of 20 MPa for improving the adherence of the cathode mixture onto the aluminum foil current collector. The weight of active material in the electrode sheet was about 4.0 mg cm^{-2}. After drying in vacuum at 120 °C for 12 h, the electrode was assembled into the coin-type cell (CR 2025) in an Ar-filled glove box. Counter electrode was pure metallic lithium sheet. A solution of 50 vol.% ethylene carbonate (EC), 50 vol.% dimethyl carbonate (DMC) and 1 M $LiPF_6$ was used as the electrolyte solution and a polypropylene (PP) film (Cellgard 2300) as the separator.

The electrochemical properties of the $LiCo_{1/6}Mn_{11/6}O_4$ electrode were measured by cycling the cell with the cut-off voltages of 3.5 and 4.4 V (*vs.* Li/Li^+) under a specific current density on a 16-channel secondary battery performance test device (BS-9300 K, Guangzhou Qingtian). A nominal specific capacity of 148 mAh g^{-1} was assumed to convert the current density into the C rate. The cyclic voltammetry measurements of the electrode were performed using a CHI 660B electrochemical workstation with a scan rate of 0.1 mV s^{-1} between 3.5 and 4.4 V (*vs.* Li/Li^+). The changes in crystal structure of the $LiCo_{1/6}Mn_{11/6}O_4$ material at various charge states during the initial charge process were investigated by ex situ XRD technique. The cells were opened in an Ar-filled glove box and the electrodes were covered by a layer of polyethylene film in order to minimize the air exposure and were transferred to the XRD analysis chamber. XRD date of $LiCo_{1/6}Mn_{11/6}O_4$ electrodes were collected in the range of $2\theta = 15–80°$ with a step of 0.04°.

3. Results and discussion

Fig. 1 shows the XRD pattern of the as-synthesized $LiCo_{1/6}Mn_{11/6}O_4$ powders. All peaks are sharp and well defined, suggesting that the synthesized compound is well crystallized. The XRD pattern is identified as a single-phase spinel structure with a space group Fd3m in which the lithium ions occupy the tetrahedral (8a) sites and manganese and cobalt ions reside at the octahedral (16d) sites. The SEM image of the $LiCo_{1/6}Mn_{11/6}O_4$ powders is shown in Fig. 2a. The particles exhibit uniform size distribution with sizes of about 100–200 nm and have good cubic structure shapes. The well-dispersed particles are due to the homogenous precursor prepared by the spray-drying technology. As shown in Fig. 2b, the precursor powder is composed of isolated spherical particles. The reason is that the spray-drying process provided a uniform heating environment which shortened the synthesizing time and overcame the agglomeration of particles.

The cyclic voltammograms (CVs) of the $LiCo_{1/6}Mn_{11/6}O_4$ electrode measured at 25 and 55 °C are shown in Fig. 3. The electrode was cycled in the potential range of 3.5–4.4 V at a scan rate of 0.1 mV s^{-1}. The CV of the electrode at 25 °C (Fig. 3a) shows two pairs of well-defined redox peaks, centered at 4.05 and 4.18 V in the charge/lithiation process and at 3.93 and 4.08 V

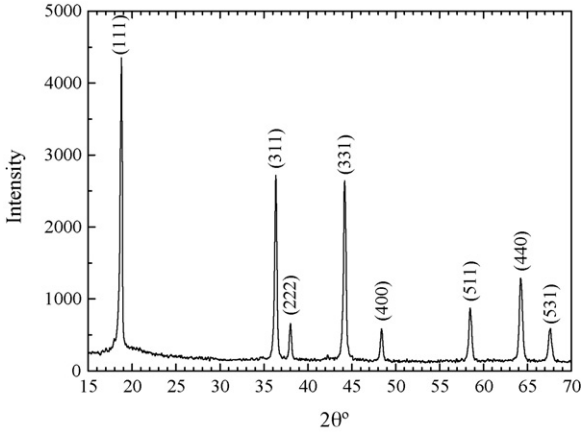

Fig. 1. XRD pattern of the as-synthesized $LiCo_{1/6}Mn_{11/6}O_4$ powders.

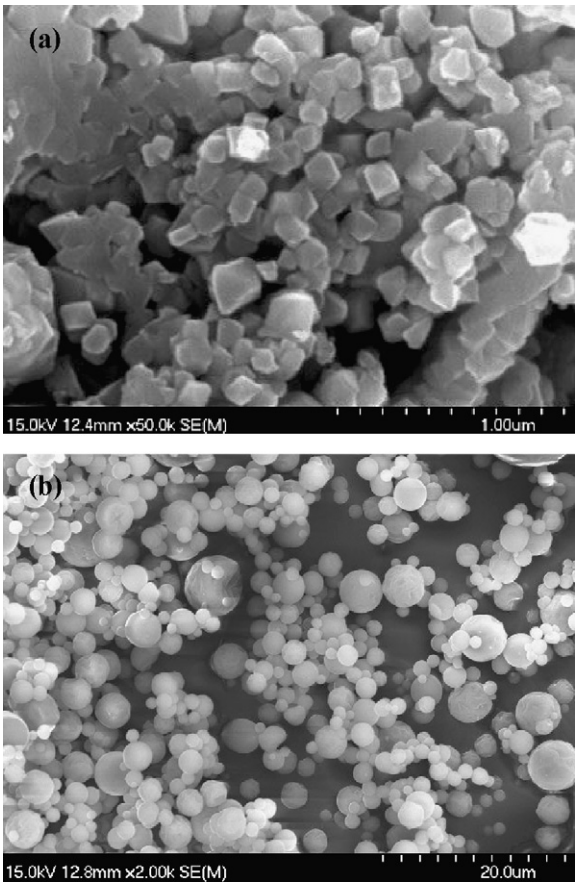

Fig. 2. SEM images of the $LiCo_{1/6}Mn_{11/6}O_4$ powders: (a) the as-synthesized $LiCo_{1/6}Mn_{11/6}O_4$ powder and (b) the precursor powder of $LiCo_{1/6}Mn_{11/6}O_4$.

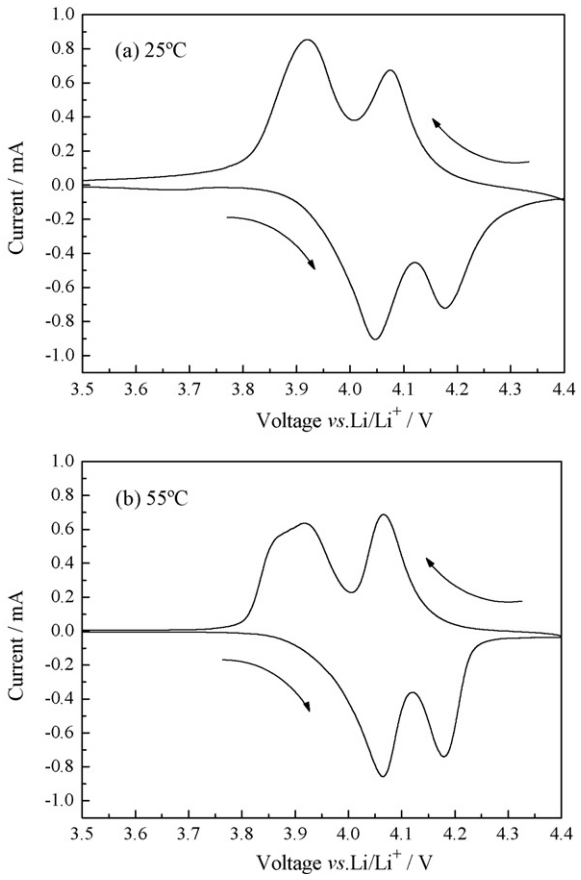

Fig. 3. Cyclic voltammograms of the $LiCo_{1/6}Mn_{11/6}O_4$ electrode at a scan rate of 0.1 mV s^{-1}: (a) 25 °C and (b) 55 °C.

in the discharge/delithiation process, respectively. The narrow redox peak potentials and the almost same redox currents illustrate a good reversibility of this material upon extraction and insertion of lithium ion. At the elevated temperature (55 °C), the peak potentials and curve shape of the CV (Fig. 3b) show no distinctive differences. It seems that the electrolyte solution is stable up to 4.4 V against the oxidation of electrode and the lithium insertion and extraction are reversible at 55 °C. Therefore, it is possible to investigate the elevated temperature properties of the $LiCo_{1/6}Mn_{11/6}O_4$ electrode ignoring the influence of electrolyte decomposition.

The initial charge/discharge curves of the $LiCo_{1/6}Mn_{11/6}O_4$ electrode ranging from 3.5 to 4.4 V at 1/10 C rate are given in Fig. 4. The differential specific capacity, dQ/dE, in units of mAh $(g\,V)^{-1}$ were calculated from adjacent points in the voltage–time data [$V(n+1)$, $V(n)$:$t(n+1)$, $t(n)$] using the known value of the current, I, and the active electrode mass, m, as follows:

$$\frac{dQ}{dE} = \frac{I[t(n+1) - t(n)]}{m[V(n+1) - V(n)]} \quad (1)$$

In these tests, when the cell voltage (V) changed by 1 mV, time (t) is measured to the nearest second. From the differential specific capacity (dQ/dE), the charge and discharge characteristics could be observed more easily.

At 25 and 55 °C, both charge and discharge curves show two clear voltage plateaus, which are a remarkable characteristic of spinel lithium manganese oxides with two-stage mechanism for the electrochemical lithium extraction and insertion. The initial discharge and charge capacity of the electrode at 25 °C are determined to be about 123 and 127 mAh g^{-1}, respectively, while for the electrode at 55 °C, the initial discharge and charge capacity are about 127 and 132 mAh g^{-1}, respectively. Both have high coulombic efficiency reaching 96%. In addition, the voltage plateaus could be approved by the curve of dQ/dE *vs.* E, since the amount of peak regions reflects that of plateaus. It is seen that each curve of dQ/dE *vs.* E has two-peak region in the corresponding curve of dQ/dE *vs.* E. The intensity of peaks for the electrode at 25 °C is slightly stronger than that for the electrode at 55 °C, indicating that the former holds better charge/discharge characteristics.

Fig. 5 shows the cycling performance of the $LiCo_{1/6}Mn_{11/6}O_4$ electrode ranging from 3.5 to 4.4 V at 1/5 C rate. At 25 °C, the $LiCo_{1/6}Mn_{11/6}O_4$ electrode delivers an initial discharge capacity of 119 mAh g^{-1} with an excellent cycling performance up to 50 cycles. At 55 °C, the $LiCo_{1/6}Mn_{11/6}O_4$ electrode shows a slightly higher initial capacity of 129 mAh g^{-1}, mainly because at the elevated temperature, the lithium insertion and extraction maybe start more easily, and the electrode can be wetted by the electrolyte more quickly. The cell also cycles well with a limited capacity fade after 50 cycles. The capacity fading rate is 0.107% per cycle at 25 °C, and 0.302% per cycle at 55 °C, respectively. As compared to $LiCo_{1/6}Mn_{11/6}O_4$ pre-

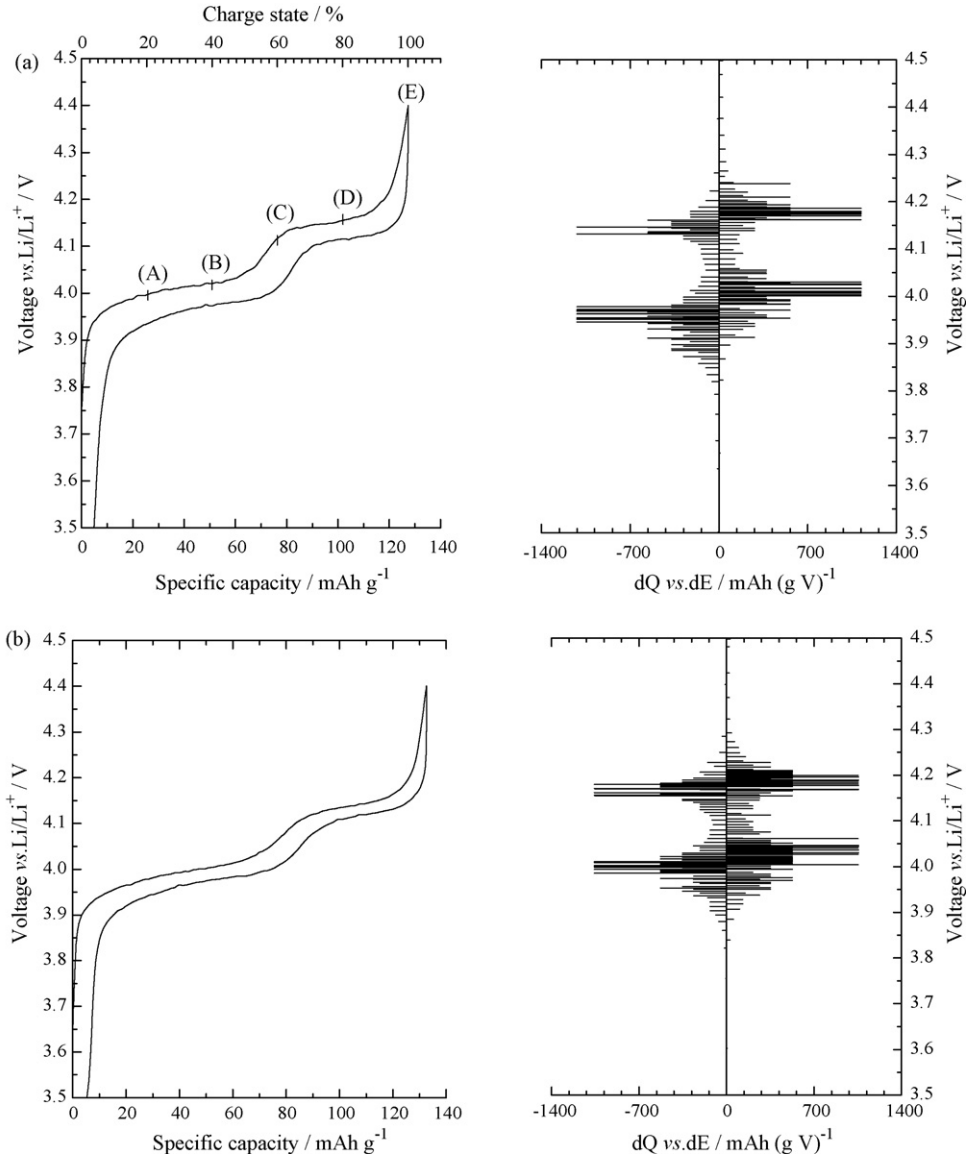

Fig. 4. The initial charge/discharge curves of the $LiCo_{1/6}Mn_{11/6}O_4$ electrode at 1/10 C rate and the corresponding dQ/dE *vs.* voltage curves: (a) 25 °C and (b) 55 °C.

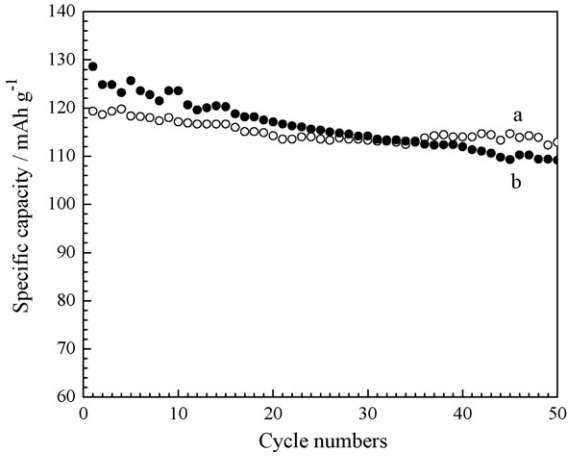

Fig. 5. Cycling performance of the $LiCo_{1/6}Mn_{11/6}O_4$ electrode at 1/5 C rate: (a) 25 °C and (b) 55 °C.

pared by the Pechini process [14], ultrasonic spray pyrolysis [21] and sol–gel [22], the cycling performance of the synthesized $LiCo_{1/6}Mn_{11/6}O_4$ by spray-drying method is greatly improved, especially at elevated temperature. The small and homogeneous particles will maximize the contacts between active material and electrolyte solution, thus improving kinetics for the lithiation/delithiation reactions. In addition, the $LiCo_{1/6}Mn_{11/6}O_4$ material has stabilized structure and can reduce strain during the repeated insertion/de-insertion of lithium.

Lithiation (discharge)/delithiation (charge) reaction into/from spinel $LiCo_{1/6}Mn_{11/6}O_4$ proceeds reversibly according to the following equation:

$$LiCo_{1/6}Mn_{11/6}O_4 - \Delta x Li^+ + \Delta x e \overset{\text{charge(delithiation)}}{\underset{\text{discharge(lithiation)}}{\rightleftarrows}} \times Li_{1-\Delta x}Co_{1/6}Mn_{11/6}O_4 \quad (2)$$

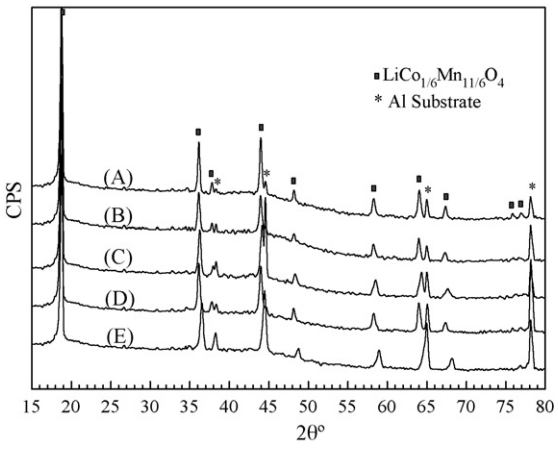

Fig. 6. XRD pattern evolution of the $LiCo_{1/6}Mn_{11/6}O_4$ electrode during the first charge process at 25 °C.

For monitoring the changes in the crystal structure during cycling, the ex situ XRD technique was conducted on the $LiCo_{1/6}Mn_{11/6}O_4$ electrodes at selected charge states at 25 °C. The points labeled (A)–(E) on the voltage profile in Fig. 4a indicate the various charge states at which, the XRD date are collected.

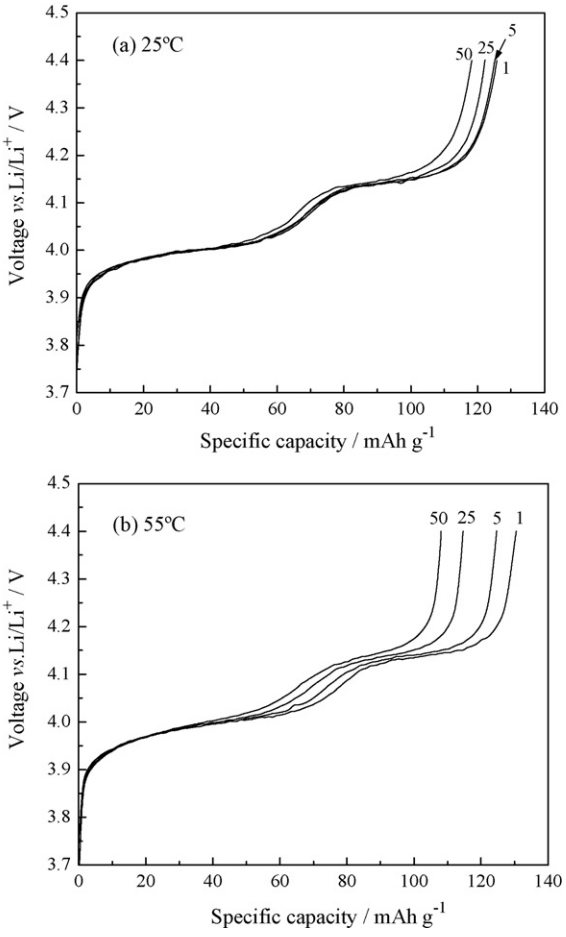

Fig. 7. Charge curves of the $LiCo_{1/6}Mn_{11/6}O_4$ electrode at the 1st, 5th, 25th and 50th cycle at 1/5 C: (a) 25 °C and (b) 55 °C.

Fig. 6 shows the ex situ XRD patterns collected at points (A)–(E) in Fig. 4a during the first charge process at 1/10 C at 25 °C. The first observation to note is that from charge state at 20% to the fully delithiated electrode (patterns (A)–(E)), the peak locations have some excursion. They shift continuously to higher diffraction angles with decreasing the Li-content in the $LiCo_{1/6}Mn_{11/6}O_4$ electrodes. From patterns (C)–(E), the change of degree of 2θ is larger than that from patterns (A)–(C), which can be attributed to a little more lithium ion being extracted in the high-voltage range. Moreover, there are not any new other peaks appeared. It is suggested that the material configuration has not be destroyed and the crystal structure of the $LiCo_{1/6}Mn_{11/6}O_4$ material is stable during charge process.

As shown in Fig. 4, the spinel structure $LiCo_{1/6}Mn_{11/6}O_4$ presents two voltage plateaus during the charge and discharge process. In order to study the stability of capacity at different operating temperatures, the charge curves of the $LiCo_{1/6}Mn_{11/6}O_4$ electrode at the 1st, 5th, 25th and 50th cycle at 1/5 C are plotted in Fig. 7. For the electrode cycled at 55 °C, there is a little capacity loss in the low-voltage region (3.50–4.08 V), and the capacity fade occurs mainly in the high-voltage region (4.08–4.40 V). This result indicates that the structure of $LiCo_{1/6}Mn_{11/6}O_4$ in the low-voltage region is more stable for Li-ion insertion/de-insertion at the elevated temperature. By contrast, the electrode operated at 25 °C exhibits less capacity loss in the high-voltage region, and as well as in the low-voltage region. The phenomena may be ascribed to the dissolution of the Mn^{3+} into the electrolyte solution. The elevated temperature condition accelerates the process of Mn dissolution.

4. Conclusions

Sub-micro spinel $LiCo_{1/6}Mn_{11/6}O_4$ powders were prepared by a spray-drying method. The as-prepared powders were identified as a single-phase spinel with Fd3m space group and had a uniform particle size distribution and high degree of crystallization. It delivered high initial discharge capacities of 123 and 127 mAh g^{-1} at 1/10 C rate ranging from 3.5 to 4.4 V at 25 and 55 °C, respectively. At these temperatures, it both showed good cycle stability at 1/5 C rate. The capacity fading rate was 0.107% per cycle at 25 °C, and 0.302% per cycle at 55 °C, respectively. In the charge/discharge process, the capacity fading occurred mainly in the high-voltage region, especially at high operating temperature. An ex situ XRD displayed the spinel material configuration maintained stabilization during cycling.

Acknowledgement

This work was supported by the National Natural Science Foundation of China (No. 50402020).

References

[1] J.M. Tarascon, E. Wang, F.K. Shokoohi, W.R. McKinnon, S. Colson, J. Electrochem. Soc. 138 (1991) 2859–2864.
[2] M.M. Thackeray, P.J. Johnson, L.A. de Picciotto, P.G. Bruce, J.B. Goodenough, Mater. Res. Bull. 19 (1984) 179–187.

[3] M.M. Thackeray, L.A. de Picciotto, A. de Kock, P.J. Johnson, V.A. Nicholas, K.T. Adendorff, J. Power Sources 21 (1987) 1–8.
[4] Y. Xia, N. Kumada, M. Yoshio, J. Power Sources 90 (2000) 135–138.
[5] R.J. Gummow, A. de Kock, M.M. Thackeray, Solid State Ionics 69 (1994) 59–67.
[6] L. Guohua, H. Ikuta, T. Uchida, M. Wakihara, J. Electrochem. Soc. 143 (1996) 178–182.
[7] X. Wu, S. Bin Kim, J. Power Sources 109 (2002) 53–57.
[8] G.T.K. Fey, C.Z. Lu, T.P. Kumar, J. Power Sources 115 (2003) 332–345.
[9] L. Hernán, J. Morales, L. Sánchez, J. Santos, Solid State Ionics 118 (1999) 179–185.
[10] P. Arora, B.N. Popov, R.E. White, J. Electrochem. Soc. 145 (1998) 807–815.
[11] J.M. Amarilla, J.L. Martín de Vidales, R.M. Rojas, Solid State Ionics 127 (2000) 73–81.
[12] M. Okada, Y.S. Lee, M. Yoshio, J. Power Sources 90 (2000) 196–200.
[13] C.H. Shen, R.S. Liu, R. Gundakaram, J.M. Chen, S.M. Huang, J.S. Chen, C.M. Wang, J. Power Sources 102 (2001) 21–28.
[14] S.H. Wu, H.J. Su, Mater. Chem. Phys. 78 (2003) 189–195.
[15] Q. Wu, X. Li, M. Yan, Z. Jiang, Electrochem. Commun. 5 (2003) 878–882.
[16] Y. Shin, A. Manthiram, Electrochim. Acta 48 (2003) 3583–3592.
[17] T. Kakuda, K. Uematsu, K. Toda, M. Sato, J. Power Sources 167 (2007) 499–503.
[18] Y. Idemoto, H. Narai, N. Koura, J. Power Sources 119–121 (2003) 125–129.
[19] H.M. Wu, J.P. Tu, Y.F. Yuan, Y. Li, X.B. Zhao, G.S. Cao, Scripta Mater. 52 (2005) 513–517.
[20] H.M. Wu, J.P. Tu, Y.F. Yuan, Y. Li, X.B. Zhao, G.S. Cao, Electrochim. Acta 50 (2005) 4104–4108.
[21] I. Taniguchi, D. Song, M. Wakihara, J. Power Sources 109 (2002) 333–339.
[22] H.J. Bang, V.S. Donepudi, J. Prakash, Electrochim. Acta 48 (2002) 443–451.